SCIENTIFIC REPORTS

OPEN

SUBJECT AREAS:
MOLECULAR SELF-ASSEMBLY
SOFT MATERIALS

Received
11 February 2014

Accepted
7 May 2014

Published
28 May 2014

Correspondence and requests for materials should be addressed to W.J.W. (wengwj@zju.edu.cn) or W.-Q.H. (hanweiqiang@nimte.ac.cn)

* These authors contributed equally to this work.

Facet-Specific Assembly of Proteins on $SrTiO_3$ Polyhedral Nanocrystals

Lingqing Dong[1,2]*, Qi Luo[3]*, Kui Cheng[1]*, Hui Shi[3], Qi Wang[3], Wenjian Weng[1,4] & Wei-Qiang Han[1,2,5]

[1]Department of Materials Science and Engineering, State Key Laboratory of Silicon Materials, Cyrus Tang Center for Sensor Materials and Applications, Zhejiang University, Hangzhou 310027, China, [2]Ningbo Institute of Materials Technology & Engineering, Chinese Academy of Sciences, Ningbo 315210, China, [3]Soft Matter Research Center and Department of Chemistry, Zhejiang University, Hangzhou 310027, China, [4]Shanghai Institute of Ceramics, Chinese Academy of Sciences, Shanghai 200050, China, [5]School of Physical Science and Technology, ShanghaiTech University.

Precisely controlling the protein-nanomaterial interactions at selective sites is crucial in engineering biomolecule composite architectures with tailored nanostructures and functions for a variety of biomedical applications. This strategy, however, is only beginning to be explored. Here, we demonstrate the facet-specific assembly of proteins, such as albumin, immunoglobulin and protamine, on {100} facets of $SrTiO_3$ polyhedral nanocrystals, while none on {110} facets. Molecular dynamics simulations indicate the immobile surface hydration layer might play a barrier role to effectively prevent proteins adsorption on specific {110} facets. This work thus provides new insights into the fundamentally understanding of protein-nanomaterial interactions, and open a novel, general and facile route to control the selective adsorption of various proteins on various nanocrystals.

Over the past decade, the use of nanoparticles in biological applications, such as drug deliver[1,2], biosensing[3,4], as well as medical imaging, has been experienced an explosion of scientific interest because of their intrinsic size- and facet-dependent properties as well as functional properties[3–5]. The small size of nanoparticles confers them high specific surface areas and penetrability through many biological pathways resulting in high interaction with biological structures. When nanoparticels enter a biological fluid (for example blood, human plasma or interstitial fluid), a process of non-specific adsorption of protein onto the surface of nanoparticles immediately occurs, thus forming a nanoparticle-protein corona, which affects how nanoparticles are internalized by cells and cleared from the body[6]. Therefore, rational design the nanoparticles can offer tremendous opportunities in terms of engineering the nanoparticle-protein interactions[7]. For example, monolayer-protected metal nanoparticles, with ligand shell, can regulate cell-membrane penetration by preventing non-specific adsorption of proteins[8,9]. Polyethylene oxide-functionalized carbon nanotube-based biosensors have been used for selective recognition of target proteins[10]. In recent years, considerable efforts have been put into understanding the distribution of reacted sites for protein adsorption[11–13]. However, how to precisely and selectively engineer protein to a specific site is still a challenge.

Some progresses for site-selective adsorption of protein on flat substrate have been reached by using traditional photolithographic processes[14], which are not applicable to the nonplanar objects and challenging in scaling down the objects to submicrometer size scale[15]. Researchers have shown that size-related surface curvature and protein structure influence protein orientation on silica nanoparticles[16]. Bimetallic nanowires composed of gold and nickel segments functionalized with alkanethiols with terminal hexa(ethylene glycol) groups(EG_6) and palmitic acid, a 16-carbon fatty acid, respectively, have exhibited different fluorescence behavior when exposed to a fluorescently tagged protein. Intense fluorescence was only observed on the nickel segment of these wires. However, the localization of two functionalities on different regions of the nanowire cannot be easily mimicked with spherical nanoparticles[17]. Moreover, additional functionality means additional synthetic steps and costs, more complicated behavior and effects in vivo[18]. The spatial selective adsorption of protein on specific surfaces of a non-functional single nanoparticle has yet to be demonstrated. Nanocrystals with well-controlled shapes and selectively exposed facets could be a model system to better understand the mechanisms of nanoparticle-cell interactions.

Here we demonstrate the selective adsorption of proteins, such as bovine serum albumin (BSA), porcine immunoglobulin G (IgG) and salmine, on {100} facets of $SrTiO_3$ polyhedral nanocrystals, while none on {110} facets.

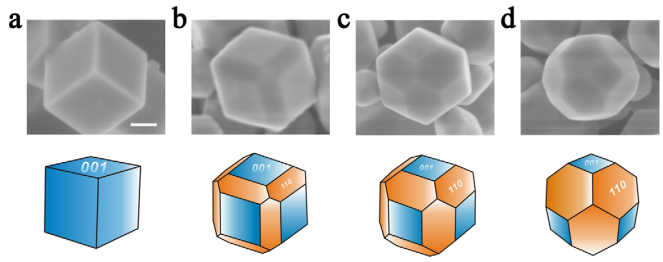

Figure 1 | Shape-controlled synthesis of $SrTiO_3$ nanocrystals. SEM images and the corresponding schematic drawings of $SrTiO_3$ nanocrystals synthesized with morphology evolution from cube to truncated rhombic dodecahedron upon the increasing addition of 1,3-propanediol from (a) 0 ml to (b) 1 ml, (c) 3 ml and (d) 5 ml. Scale bar, 100 nm.

Results and discussions

Shape-controlled $SrTiO_3$ polyhedral nanocrystals are synthesized by using titanium tetrachloride ($TiCl_4$) aqueous solution and strontium chloride ($SrCl_2$) as the titanium precursor and strontium source, respectively, as well as 1,3-propanediol as a surfactant. Figure 1 presents scanning electron microscopy (SEM) images and the corresponding drawings of the $SrTiO_3$ polyhedral nanocrystals synthesized by varying 1,3-propanediol concentrations (Supplementary Figure S1 shows low-magnification SEM images). By progressively increasing the concentration of 1,3-propanediol added to the reaction mixture solution (from 0 to 0.2 M, 0.6 M and 1 M), a systematic shape evolution from cube to truncated rhombic dodecahedron is successfully achieved. We consider that the mechanism behind these results can be explained by "kinetic and thermodynamic modified Wulff constructions" developed by Ringe, E. et al.[19]. The cube is bounded by six identical {100} facets while the truncated rhombic dodecahedron is bounded by six square {100} facets and twelve hexagonal {110} facets, which are confirmed by transmission electron microscopy (TEM) and selected-area electron diffraction (SAED) analysis (Supplementary Figure S2). The average particle sizes for the cube and truncated rhombic dodecahedron are 238 nm, 228 nm, 183 nm and 177 nm with relative standard deviations of 11%, 12%, 8% and 7%, respectively (Supplementary Figure S1).

Supplementary Figure S3 shows X-ray diffraction (XRD) spectra of the four samples. The resulted diffraction patterns match very well with the crystal structure of cubic $SrTiO_3$ (JCPDS No. 73-0661). Interestingly, a close examination shows that the increase of ratio of diffraction peak intensity $I_{(220)}/I_{(200)}$ from 0.31 for the cube to 0.37, 0.43, and 0.47 for the series of truncated rhombic dodecahedra, indicating the increasing of the exposed {110} facets ratio[20,21].

To study the adsorption behavior of proteins on $SrTiO_3$ polyhedral nanocrystals, we put truncated rhombic dodecahedral $SrTiO_3$ nanocrystals, which contained both {100} and {110} facets, into protein solution. Figure 2 shows SEM images of typical $SrTiO_3$ truncated rhombic dodecahedra after treated by proteins, respectively. Surprisingly, all the proteins achieve high packing density on the {100} facets of truncated rhombic dodecahedra, while {110} facets adsorb nothing. To determine the adsorption of protein on nanocrystals, we compare the concentration of protein before/after adsorption by measuring the optical density (OD) values. In comparison of A and B in Supplementary Figure S4, the constant of OD values of the protein solution without addition of nanocrystals before/after centrifugation indicates that protein can not be centrifuged down. In contrast, the OD values of the protein solution (the supernatant after centrifugation) with addition of nanocrystals significantly decrease, which suggest the adsorption of protein on nanocrystals. Evidence for the adsorption of salmine on $SrTiO_3$ nanocrystals is also obtained by Fourier transform infrared (FTIR) experiments. As shown in Figure 3b, the adsorption bands appeared at 1660 cm^{-1} (C=O stretching vibration) and 1541 cm^{-1} (N-H

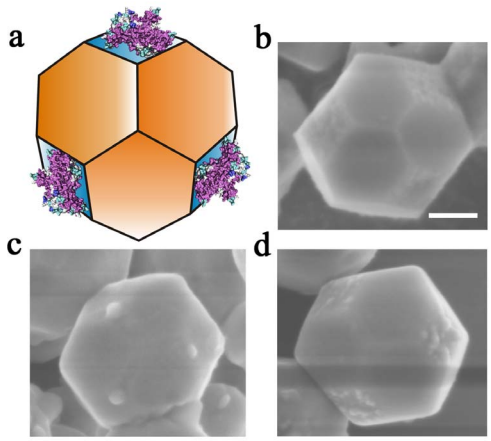

Figure 2 | Schematic illustration and SEM images of truncated rhombic dodecahedra $SrTiO_3$ nanocrystals after adsorption of proteins. (a) schematic illustration of the selective adsorption of proteins on $SrTiO_3$ {100} facets, (b) bovine serum albumin (BSA), (c) porcine immunoglobulin G (IgG) and (d) salmine. Scale bar, 100 nm.

bending vibration mainly, coupled to C=O and C=C stretching) of salmine are characteristic amide I and amide II bands, respectively. The band at 1452 cm^{-1} can be attributed to CH_2 and CH_3 groups. The band at 1242 cm^{-1} is consistent with the canonical values for β-sheet conformation[22,23]. And the intense band at 1084 cm^{-1} can be attributed to the arginine of salmine[24]. By comparison with the spectra of salmine after adsorption on $SrTiO_3$ nanocrystals (Figure 3a), the shift of amide I adsorption band to 1655 cm^{-1} (α-helices), which is also attributed to the carbonyl stretching frequency to interaction with the surface[25], and the diminishing of the bands at 1452 cm^{-1} and 1242 cm^{-1} as well as the increase in the ratios of amide I/amide II, suggest a strong interaction of salmine with $SrTiO_3$ nanocrystal and thus the conformational change of protein structure[26]. Furthermore, two apparent bands at 1155 cm^{-1} and 1076 cm^{-1} in Figure 3a, which can be assigned to asymmetrical and symmetrical stretching vibration of S=O, respectively, also reflect the interaction between salmine and $SrTiO_3$ nanocrystal surface. The bands at 858 cm^{-1}, 617 cm^{-1} (also can be assigned to amide IV of protein) and 544 cm^{-1}, which are associated to the stretching of Ti-O-Ti of $SrTiO_3$ nanocrystal[27], are also observed in Figure 3a. We further investigate the facet-specific adsorption behavior of protein on

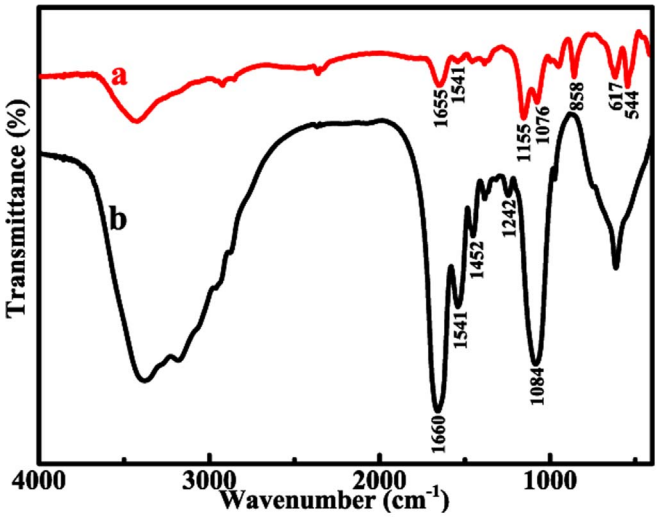

Figure 3 | FT-IR spectra of $SrTiO_3$ nanocrystals after adsorption of salmine (a) and salmine itself (b).

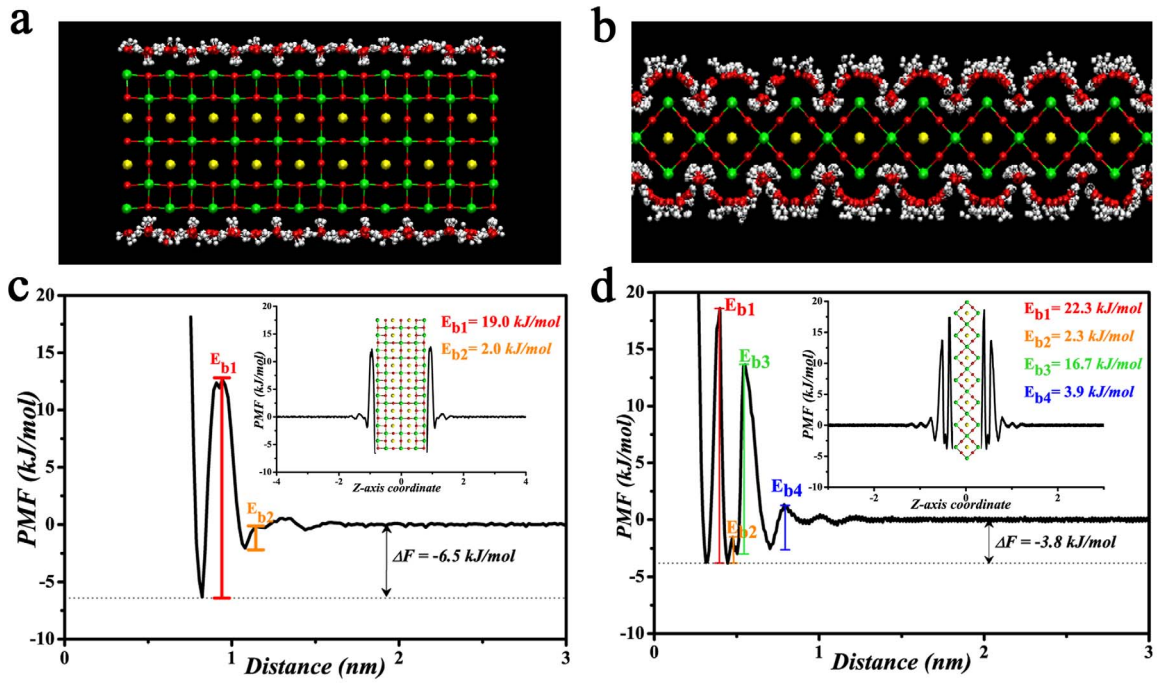

Figure 4 | MD simulations of the interfacial water structures on two facets and their calculated potential mean force (PMF). (a) {100} facet, (b) {110} facet, (c), (d) the corresponding PMF. The insets show the full profiles.

$SrTiO_3$ polyhedral nanocrystals by using high angle annular dark field scanning transmission electron microscopy (HAADF-STEM). The increased first then decreased signal of U and N elements of line-scan energy dispersive X-ray spectroscopy (EDS) profiles at the interfaces further verify the facet-selective adsorption of proteins on the {100} facets, while the {110} facets absorbed nothing, (see Supplementary Figure S5). The distinct proteins adsorption selectivity on various facets of $SrTiO_3$ polyhedral nanocrystals indicates that the facet-selectivity could be a general route to control various proteins on various nanocrystals.

According to the previous investigations of protein-nanoparticle adsorption, some factors, such as surface atomic structure, chemisorbed functional groups and adsorption conditions, affect the adsorption behavior[28–30]. Among these factors, functionalization of nanoparticles with organic molecules, such as poly(ethylene glycol) (PEG), is a popular way to reduce protein adsorption[31,32]. In this work, 1,3-propanediol, an alcohol molecules, is used during synthesis process. Infrared spectrum analysis shows that the final products have no organic residuals after calcination process. Therefore, the influence of alcohol molecules on protein-nanocrystal interaction could be ruled out. Additionally, the selective adsorption of proteins on the {100} facets of $SrTiO_3$ nanocrystals is almost not affected by other protein treatment conditions, such as temperature and solvent, based on the comparative experiments carried out at different temperature and using water as the solvent, respectively.

Since the above mentioned factors are not responsible for the distinct protein adsorption selectivity on {100} and {110} facets of $SrTiO_3$ polyhedral nanocrystals, it is reasonable for us to point the origin of the selectivity is the facet-selective protein adsorption, which is related to intrinsic difference of the surface atomic structures of the {100} and {110} facets of $SrTiO_3$. Chiu et al. reported that facet-selective binding peptides as regulating agents for the synthesis of Pt nanocrystals with selectively exposed facets[33]. When conjugated with a-chymotrypsin (ChT), the estimated surface coverage of Au nanocube with {100} facets is 1–2 times more than that of Au nanooctahedra with {111} facets[34]. These previous reports have large difference from the present results that the protein fully cover {100} facets of $SrTiO_3$ nanocrystals, but none for {110} facets. Furthermore, fundamental understanding of protein-nanoparticle interaction mechanism at the molecular-level is largely incomplete and under considerable debate. Our Molecular Dynamic (MD) simulations of BSA adsorption on {100} and {110} facets of $SrTiO_3$ only predict that former has higher protein coverage probability than the latter, which does not describe the fact of no protein-coverage on {110} facets. Some researchers have suggested that the formation of structured or tightly bound water at the interface may play a critical role in determining surfaces for their ability of adsorption of proteins from solution because the interfacial water molecules provide a physical barrier preventing direct contact between protein and surface[35–38]. Theoretical modeling for the structure of interfacial water molecules onto surfaces also helps better understanding of protein adsorption behavior[39–41]. To gain insight into the facet-selective adsorption of proteins onto the facets of $SrTiO_3$ nanocrystals, we carried out atomistic MD simulations to explore the structures of the interfacial water molecules onto the {100} and {110} facets of $SrTiO_3$.

Figure 4a, b show the interfacial water structures on the {100} and {110} facets of $SrTiO_3$ according to the trajectory of the last nanosecond in each system. The interfacial water structures are highly influenced by the underlying nanocrystal's atomic structures. For the {100} facet, a random arrangement of interfacial water molecules on the surface is observed, as shown in Figure 4a. On the other hand, for {110} facet, water molecules are capable of entering the lattice structure of $SrTiO_3$ by occupying the Sr atomic vacancies with highly ordered orientation and forming a water "shell" on the {110} facet of $SrTiO_3$, as illustrated in Figure 4b. The distinct difference in the behavior of the $SrTiO_3$ water interface can be attributed to the difference of surface atomic structure of the {100} and {110} facets. Interestingly, the water structures with highly ordered orientation are tightly bounded on {110} facet, i.e. forming a stable surface hydration layer, which is supported by the potential of mean force (PMF) for stability calculations for water molecules transferring from $SrTiO_3$ surface into bulk water (Figure 4c, d). The calculation results show that the free energy (ΔF) for bulk water molecules transferring to the surface of {100} facet (−6.5 kJ/mol) is comparable to that of {110} facet (−3.8 kJ/mol), which suggests that thermodynamical stability of the water layers on the {100} and {110} facets has no

significant difference. Surprisingly, the energy barriers (E_b) relevant to the {100} and {110} facets exhibit great difference. There are four energy barriers for the water molecules transferring from $SrTiO_3$ {110} facet into bulk water and the barrier height (E_{b1}, 22.3 kJ/mol; E_{b2}, 2.3 kJ/mol; E_{b3}, 16.7 kJ/mol; E_{b4}, 3.9 kJ/mol) is remarkably higher than that from {100} facet (E_{b1}, 19.0 kJ/mol; E_{b2}, 2.0 kJ/mol) (Figure 4c, d), which indicates that the interfacial water structures on the {110} facet is far more still than that on the {100} facet. According to the experimental observations by Chou et al.[42] and the theoretical calculations by Jiang et al.[43], the immobile surface hydration layer plays a role of barrier to effectively prevent protein adsorption, which can explain much stronger protein adsorption affinity for the {100} facet in our experimental results, selective protein adsorption on the {100} facet, but none on the {110} facet. The MD simulations provide detailed insights into the role of the interfacial water in determining the protein adsorption behavior.

Conclusions

In summary, the proteins, such as bovine serum albumin (BSA), porcine immunoglobulin G (IgG) and salmine, attain high packing density on the {100} facets of truncated rhombic dodecahedra, while {110} facets adsorb nothing. The distinctly different proteins adsorption behavior between the {100} and {110} facets of $SrTiO_3$ might be attributed to the distinctly different behavior of water molecules-binding properties of these two facets. Molecular dynamics (MD) simulations indicate the immobile surface hydration layer might play a role of barrier to effectively prevent protein adsorption on specific {110} facet. The distinct proteins adsorption selectively on the facets of $SrTiO_3$ polyhedral nanocrystals indicates that the facet-selectivity could be a general route to control other proteins on the other nanocrystals.

Methods

Synthesis of $SrTiO_3$ nanocrystals. In a typical synthesis, 0.265 ml of $TiCl_4$ (aladdin, 99%) solution is dropwised into 25 ml of the 1,3-propanediol solution that is cooled in an ice bath. After stirring for 5 min, 30 ml of 3 M LiOH (aladdin, 98%)solution and 10 ml of 0.24 M $SrCl_2$ (aladdin, 99.5%) solution are added subsequently. After stirring for another 30 min, the resulting solution is transferred to a Teflon-lined autoclave and heat at 180°C for 48 h. After the reaction, the resulted precipitate is centrifuged and rinsed using water and ethanol, then dried at 70°C for 12 h. Finally, the dried samples are heated at 600°C to remove organic residue.

Adsorption of proteins on $SrTiO_3$ nanocrystals. We selected simple cubic perovskite oxide $SrTiO_3$ nanocrystals as model, since its surface atomic-level and electronic structure has attracted continuing interest[44,45], and thus can facilitate our understanding the facet-dependent protein adsorption behavior. To investigate the adsorption of proteins to the facets of $SrTiO_3$ nanocrystals, 1 ml of 5 mg/ml $SrTiO_3$ nanocrystals solution is added to 5 ml 1 g/l protein solution in phosphate buffered saline (PBS, pH 7.4) at 37°C for 12 h. The collected sample is centrifuged and then dried at ambient air.

MD simulations of the interfacial water structures on {100} and {110} facets. Considering that the atomic surface structures of $SrTiO_3$ nanocrystals are synthesis dependent[46], we use spherical aberration (Cs) corrected TEM to determine the surface atomic structures of $SrTiO_3$ (001) and (110) facets (see Supplementary Figure S6). The results indicate that the surface compositions of the atomic layer of (100) and (110) surfaces are TiO_2 double-layer[46] and a Sr deficient TiO layer[47], respectively. A 20-ns MD simulation is performed for each $SrTiO_3$ facet in water molecules system. The facets modeled slabs are set parallel to the *x*-*y* plane. Each system is immersed in a rectangular box. The box dimensions in the *x* and *y* directions fit the crystal parameters of the facets, thus creating infinite slabs in the *x*-*y* plane[40]. The boxes are filled with water molecules and the facets are frozen during the simulations. All simulations are performed in the canonical (NVT) ensemble with the Gromacs program package[48]. The $SrTiO_3$ parameters are supplemented, in which the Lennard-Jones parameters of Sr, Ti and O atoms are obtained from fitting to the Buckingham potentials (Supplementary Table S1)[49]. For the water molecules, the SPC/E (extended simple point charge model) model is employed[50]. The particle mesh Ewald method is used to describe the long-range electrostatic interactions with a cutoff of 12 Å[51]. Lennard-Jones interactions are truncated between 10 Å and 11 Å with a smooth switching of the potential. The temperature is maintained at 310 K by using a Nose-Hoover thermostat[52]. A time step of 2 fs is used and the trajectories are saved every 10 ps for analysis. To calculate the potential of mean force (PMF) of water molecules, the probability distribution of water molecules (approximately represented by the oxygen atoms) $g(\xi)$ along *z*-axis direction is calculated using Eq. (1): $g(\xi) = <\rho(\xi)>/<\rho>$, where $<\rho(\xi)>$ is the local density of the water molecules at the *z*-axis coordinate ξ, and $<\rho>$ is the bulk density of water molecules. Then PMF(ξ) is calculated based on $g(\xi)$ using Eq.(2): $PMF(\xi) = -RT \ln g(\xi)$.

1. Goldberg, M. S. *et al.* Nanoparticle-mediated delivery of sirna targeting parp1 extends survival of mice bearing tumors derived from brca1-deficient ovarian cancer cells. *Proc. Natl Acad. Sci. USA* **108**, 745–750 (2011).
2. Duncan, B. *et al.* Gold nanoparticle platforms as drug and biomacromolecule delivery systems. *J. Controlled Release* **148**, 122–127 (2010).
3. Kim, D. *et al.* Antibiofouling polymer-coated gold nanoparticles as a contrast agent for in vivo x-ray computed tomography imaging. *J. Am. Chem. Soc.* **129**, 7661–7665 (2007).
4. von Maltzahn, G. *et al.* Computationally guided photothermal tumor therapy using long-circulating gold nanorod antennas. *Cancer Res.* **69**, 3892–3900 (2009).
5. Park, J.-H. *et al.* Biodegradable luminescent porous silicon nanoparticles for in vivo applications. *Nat. Mater.* **8**, 331–336 (2009).
6. Nel, A. E. *et al.* Understanding biophysicochemical interactions at the nano-bio interface. *Nat. Mater.* **8**, 543–557 (2009).
7. Gagner, J. E. *et al.* Engineering nanomaterials for biomedical applications requires understanding the nano-bio interface: A perspective. *J. Phys. Chem. lett.* **3**, 3149–3158 (2012).
8. Verma, A. *et al.* Surface-structure-regulated cell-membrane penetration by monolayer-protected nanoparticles. *Nat. Mater.* **7**, 588–595 (2008).
9. Jackson, A. M. *et al.* Spontaneous assembly of subnanometre-ordered domains in the ligand shell of monolayer-protected nanoparticles. *Nat. Mater.* **3**, 330–336 (2004).
10. Chen, R. J. *et al.* Noncovalent functionalization of carbon nanotubes for highly specific electronic biosensors. *Proc. Natl Acad. Sci. USA* **100**, 4984–4989 (2003).
11. Hakem, I. F. *et al.* Understanding ligand distributions in modified particle and particlelike systems. *J. Am. Chem. Soc.* **132**, 16593–16598 (2010).
12. Mullen, D. G. *et al.* A quantitative assessment of nanoparticle-ligand distributions: Implications for targeted drug and imaging delivery in dendrimer conjugates. *Acs Nano* **4**, 657–670 (2010).
13. Meder, F. *et al.* Controlling protein-particle adsorption by surface tailoring colloidal alumina particles with sulfonate groups. *Acta Biomater.* **9**, 5780–5787 (2013).
14. Wong, L. S. *et al.* Selective covalent protein immobilization: Strategies and applications. *Chem. Rev.* **109**, 4025–4053 (2009).
15. Chen, H.-Y. *et al.* Colloids with high-definition surface structures. *Proc. Natl Acad. Sci. USA* **104**, 11173–11178 (2007).
16. Shrivastava, S. *et al.* Position-specific chemical modification and quantitative proteomics disclose protein orientation adsorbed on silica nanoparticles. *Nano. Lett.* **12**, 1583–1587 (2012).
17. Birenbaum, N. S. *et al.* Selective noncovalent adsorption of protein to bifunctional metallic nanowire surfaces. *Langmuir* **19**, 9580–9582 (2003).
18. Cheng, Z. *et al.* Multifunctional nanoparticles: Cost versus benefit of adding targeting and imaging capabilities. *Science* **338**, 903–910 (2012).
19. Ringe, E. *et al.* Kinetic and thermodynamic modified wulff constructions for twinned nanopaticles. *J. Phys. Chem. C* **117**, 15859–15870 (2013).
20. Huang, W.-C. *et al.* Synthesis of CuO_2 nanocrystals from cubic to rhombic dodecahedral structures and their comparative photocatalytic activity. *J. Am. Chem. Soc.* **134**, 1261–1267 (2012).
21. Huang, M. H. *et al.* Facet-dependent properties of polyhedral nanocrystals. *Chem. Commun.* **50**, 1634–1644 (2014).
22. Susi, H. *et al.* Infrared spectroscopy-Conformation. *Methods Enzymol.* **26**, 445–472 (1972).
23. Miyazawa, T. *et al.* Infrared spectra of polypeptides in various conformations: amide I and II bands. *J. Am. Chem. Soc.* **83**, 712–719 (1961).
24. Awotwe-Otoo, D. *et al.* Physicochemical Characterization of Complex Drug Substances: Evaluation of Structural Similarities and Differences of Protamine Sulfate from Various Sources. *AAPS. J.* **14**, 619–626 (2012).
25. Morrissey, B. W. *et al.* The conformation of adsorbed blood proteins by infrared bound fraction measurements. *J. Coll. Inferf. Sci.* **46**, 152–164 (1974).
26. McClellan, S. J. & Franses, E. I. Adsorption of bovine serum albumin at solid/aqueous interfaces. *Colloid Surf. A-Physicochem. Eng. Asp.* **260**, 265–275 (2005).
27. Jiang, Y. J. *et al.* Preparation of protamine-titania microcapsules through synergy between layer-by-layer assembly and biomimetic mineralization. *Adv. Funct. Mater.* **19**, 150–156 (2009).
28. Mahmoudi, M. *et al.* Protein-nanoparticle interactions: Opportunities and challenges. *Chem. Rev.* **111**, 5610–5637 (2011).
29. Lynch, I. & Dawson, K. A. Protein-nanoparticle interactions. *Nano Today* **3**, 40–47 (2008).
30. Shemetov, A. A. *et al.* Molecular interaction of proteins and peptides with nanoparticles. *Acs Nano* **6**, 4585–4602 (2012).
31. Zheng, M. *et al.* Ethylene glycol monolayer protected nanoparticles for eliminating nonspecific binding with biological molecules. *J. Am. Chem. Soc.* **125**, 7790–7791 (2003).
32. Larson, T. A. *et al.* Preventing protein adsorption and macrophage uptake of gold nanoparticles via a hydrophobic shield. *Acs Nano* **6**, 9182–9190 (2012).
33. Chiu, C.-Y. *et al.* Platinum nanocrystals selectively shaped using facet-specific peptide sequences. *Nat. Chem.* **3**, 393–399 (2011).

34. Gagner, J. E. *et al.* Effect of gold nanoparticle structure on the conformation and function of adsorbed proteins. *Biomaterials* **33**, 8503–8516 (2012).
35. Chapman, R. G. *et al.* Surveying for surfaces that resist the adsorption of proteins. *J. Am. Chem. Soc.* **122**, 8303–8304 (2000).
36. Raschke, T. M. Water structure and interactions with protein surfaces. *Curr. Opin. Struct. Biol.* **16**, 152–159 (2006).
37. Kane, R. S. *et al.* Kosmotropes form the basis of protein-resistant surfaces. *Langmuir* **19**, 2388–2391 (2003).
38. Kitano, H. *et al.* Structure of water in the vicinity of phospholipid analogue copolymers as studied by vibrational spectroscopy. *Langmuir* **19**, 10260–10266 (2003).
39. Israelachvili, J. & Wennerstrom, H. Role of hydration and water structure in biological and colloidal interactions. *Nature* **379**, 219–225 (1996).
40. Kang, Y. *et al.* On the mechanism of protein adsorption onto hydroxylated and nonhydroxylated TiO_2 surfaces. *J. Phys. Chem. C* **114**, 14496–14502 (2010).
41. Skelton, A. A. *et al.* Interplay of sequence, conformation, and binding at the peptide-titania interface as mediated by water. *ACS Appl. Mater. Interfaces* **1**, 1482–1491 (2009).
42. Leung, B. O. *et al.* Role of interfacial water on protein adsorption at cross-linked polyethylene oxide interfaces. *Langmuir* **28**, 5724–5728 (2012).
43. He, Y. *et al.* Origin of repulsive force and structure/dynamics of interfacial water in oeg-protein interactions: A molecular simulation study. *Phys. Chem. Chem. Phys.* **10**, 5539–5544 (2008).
44. Enterkin, J. A. *et al.* A homologous series of structure on the surface of $SrTiO_3$ (110). *Nat. Mater.* **9**, 245–248 (2010).
45. Kienzle, D. M. *et al.* Surface transmission electron diffraction for $SrTiO_3$ surfaces. *CrystEngComm* **14**, 7833–7839 (2012).
46. Lin, Y. Y. *et al.* Synthesis-dependent atomic surface structure of oxide nanoparticles. *Phys. Rev. Lett.* **111**, 156101 (2013).
47. Biswas, A. *et al.* Universal ti-rich termination of atomically flat $SrTiO_3$ (001), (110), and (111) surfaces. *Appl. Phys. Lett.* **98**, 051904 (2011).
48. Van der Spoel, D. *et al.* Gromacs: Fast, flexible, and free. *J. Comput. Chem.* **26**, 1701–1718 (2005).
49. Wohlwend, J. L. *et al.* Molecular dynamics simulations of $SrTiO_3$ thin-film growth from cluster deposition. *J. Phys.- Condens. Matter* **22**, (2010).
50. Berendsen, H. J. C. *et al.* Interaction models for water in relation to protein hydration. In: Intermolecular forces. *D. Reidel Publishing Company Dordrecht* 331–342 (1981).
51. Darden, T. *et al.* Particle mesh ewald - an n.Log(n) method for ewald sums in large systems. *J. Chem. Phys.* **98**, 10089–10092 (1993).
52. Nose, S. A unified formulation of the constant temperature molecular-dynamics methods. *J. Chem. Phys.* **81**, 511–519 (1984).

Acknowledgments

This work was supported by the National Basic Research Program of China (973 project, 2012CB933600), the National Natural Science Foundation of China (Grant No. 51072178, 51272228, 81071258 and 21273200). W.H. thanks the support from the Project of the Ningbo 3315 International Team. L.D acknowledges the contribution of Dr. Minmin Mao and Dr. Zhenju Shen of the Center of Electron Micoscope, Zhejiang University, for their assistance in characterization and discussion of $SrTiO_3$ surface atomic structure.

Author contributions

W.H., W.W. and L.D. conceived and designed the experiments. L.D. and K.C. carried out the experiments. L.D., K.C., W.W. and W.H. analyzed the data. Q.L., H.S. and Q.W. performed theoretical simulations. L.D., Q.L. and W.H. wrote the manuscript. All authors commented on the manuscript.

Additional information

Supplementary information accompanies this paper at http://www.nature.com/scientificreports

Competing financial interests: The authors declare no competing financial interests.

How to cite this article: Dong, L.Q. *et al.* Facet-Specific Assembly of Proteins on $SrTiO_3$ Polyhedral Nanocrystals. *Sci. Rep.* **4**, 5084; DOI:10.1038/srep05084 (2014).